



# Preparation and Characterization of Glycol Chitosan-Fe<sub>3</sub>O<sub>4</sub> Core–Shell Magnetic Nanoparticles for Controlled Delivery of Progesterone

Leena Mohammed<sup>1</sup>, Doaa Ragab<sup>1,†</sup>, Shigang Lin<sup>1</sup>, Somiraa Said<sup>2</sup>,  
Hassan Gomaa<sup>1</sup>, and Kibret Mequanint<sup>1,2,\*</sup>

<sup>1</sup>Department of Chemical and Biochemical Engineering, The University of Western Ontario, London, ON N6A 5B9, Canada

<sup>2</sup>Biomedical Engineering Graduate Program, The University of Western Ontario, London, ON N6A 5B9, Canada

Magnetic nanoparticles, such as superparamagnetic iron oxide nanoparticles (SPIONs) emerged as therapeutic and diagnostic agents due to their biocompatibility, bioselectivity, prolonged circulation, and chemical stability. The aim of this study was to develop novel polymeric-metallic hybrid nanoparticles coated with glycol chitosan (poly-(1,4-β-D-glucopyranosamine); GC) and loaded with progesterone. The crystalline nanoparticles were characterized by X-ray diffraction (XRD), Fourier transform infrared (FTIR) spectroscopy, transmission electron microscopy (TEM), scanning electron microscopy (SEM), thermo-gravimetric analysis (TGA), and vibrating sample magnetometer (VSM). Spherical-like superparamagnetic GC coated nanoparticles in the size range of 10–20 nm were prepared. Progesterone release mechanism from GC hybrid magnetic nanoparticles was investigated with the aid of mathematical models. Progesterone release kinetics was shown to differ significantly with pH changes where GC-coated superparamagnetic nanoparticles (Fe<sub>3</sub>O<sub>4</sub>-GC) exhibited swelling at pH 6.5 and shrinkage at pH 7.4. Moreover, metabolic activity assay of C3H10T1/2 cell line cultured with SPION-GC indicated biocompatibility of the magnetic nanoparticles. Taken together, polymeric-metallic hybrid nanoparticles have shown to be a promising nanocarrier system for controlled drug delivery applications.

**Keywords:** Superparamagnetic Iron Oxide Nanoparticles, Glycol Chitosan, Controlled Drug Delivery, pH-Responsive.

## 1. INTRODUCTION

Due to their magnetic properties and their ability to function at both cellular and molecular levels, the use of magnetic nanoparticles (MNPs) is rapidly growing for biomedical applications such as drug delivery, magnetic resonance imaging, gene delivery, fluid hyperthermia treatment, and tissue engineering.<sup>1–3</sup> MNPs have desirable physical and biological features including biocompatibility, injectability, high magnetic flux density, and narrow particle size distribution.<sup>1,4,5</sup> In drug delivery application the main advantages of MNPs are their capability to integrate drug payloads with different solubility, and the improvement in the longevity and stability of the therapeutics in the circulation.<sup>3,6</sup>

Superparamagnetic iron oxide nanoparticles (SPIONs), a main class of MNPs, have high magnetization in an AC magnetic field that can be demolished once the

field is removed. This unique property coupled with less sensitivity to oxidation and recyclability by iron metabolism through normal biochemical pathways makes them attractive for biomedical applications. The effectiveness of SPIONs is strongly dependent on the particle size, thus controlling a monodisperse distribution of the particles is very crucial.<sup>7–9</sup> Although a size distribution between 10 to 100 nm was suggested to be desirable for SPIONs parenteral administration,<sup>8,9</sup> particle agglomeration due to magnetic dipole–dipole interactions, high surface energy and large surface area-to-volume ratio is a challenge. Stable and aggregation resistant magnetic colloidal suspension can be obtained through surface modification, which creates an electrostatic repulsion between the particles in an effort to attain close to equilibrium condition between attractive and repulsive forces.<sup>2</sup> Numerous studies on surface coating of SPIONs have been performed, such as coating with inorganic materials (e.g., silica<sup>10</sup> and gold<sup>11</sup>), polymers (e.g., dextran,<sup>12</sup> polyethylene glycol (PEG),<sup>13</sup> alginate,<sup>14</sup> chitosan<sup>15,16</sup>), and

\*Author to whom correspondence should be addressed.

<sup>†</sup>Present address: The Industrial Pharmacy Department, Faculty of Pharmacy, Alexandria University, Alexandria, Egypt.

liposomes.<sup>17</sup> Whilst these coating materials enhances the SPIONs biomaterial characteristics, each has certain drawbacks which significantly limits their use *in vivo*. Some of these disadvantages include but are not limited to: high cytotoxicity, low biocompatibility, limited physiochemical properties, and complicated and/or expensive synthesis methods. For example, silica is unstable under basic conditions and its high porosity leads to oxidation and deterioration of the magnetic core.<sup>18</sup> Natural polymers such as dextran are mechanically weak and tend to break easily restraining controlled drug release.<sup>19</sup> Although synthetic polymers such as PEG have better mechanical strength, they show non-selective adsorption due to their high porosity and they also result in corrosion of the magnetic core.<sup>20</sup>

We have previously reported on chitosan coating of SPIONs showing its ability as a good coating material in controlled drug release.<sup>21</sup> However, chitosan has low solubility and restricted ability to be applied in controlled delivery due to its structurally limited sites available for functionalization. This study aims to overcome that challenge by using a chitosan derivative (glycol chitosan (GC)), which to our knowledge had not been used as a coating material for SPIONs in drug delivery applications. The therapeutic agent chosen for this study was progesterone, a 21-carbon hydrophobic steroid female hormone that plays an important role during the reproductive cycle and is also an anti-mineralocorticoid and anti-androgenic agent.<sup>22</sup> Progesterone also showed promising results in prostate hyperplasia treatment, which otherwise leads to cancer in men.<sup>23</sup> Furthermore, it affects sleep patterns and erectile function,<sup>24</sup> and it has positive effects in the neurotransmission system and brain injuries recovery.<sup>25,26</sup> Since iron-oxide nanoparticles have shown potential in therapeutic applications,<sup>27,28</sup> their utility in controlled drug delivery is attractive.

In view of the above, the objective of this work was to investigate GC-coated SPIONs as a nano-carrier system for controlled delivery of progesterone. The proposed inorganic-polymeric hybrid nanoparticles were developed and the effect of pH on the *in vitro* release kinetics of progesterone-loaded GC-coated SPIONs was investigated.

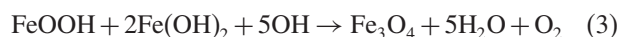
## 2. MATERIALS AND METHODS

### 2.1. Materials

The chemicals used in this study were analytical grade and were used as received without further purification. Ferrous (II) sulfate hepta-hydrate (FeSO<sub>4</sub> · 7H<sub>2</sub>O, Reagent Plus®, ≥99%) was purchased from Sigma-Aldrich (St. Louis, MO). Progesterone (MW = 314.46, ≥99%), phosphate buffered saline tablets, dialysis kit (Pur-A-Lyzer Mega 12000) with a membrane type of regenerated cellulose, and glycol chitosan (MW = 250,000, ≥60%) were purchased from Sigma-Aldrich. Ammonium hydroxide (28–30% assay) was obtained from VWR International (Mississauga, ON).

### 2.2. Preparation of Uncoated and GC-Coated SPIONs

The general approach used to prepare the magnetic nanoparticles is a modification of the co-precipitation method.<sup>21</sup> However, instead of using two iron salts (ferrous and ferric chloride), only one type of salt was used and the preparation was carried out under atmospheric conditions. These modifications resulted in an easier and less expensive method of preparation, while maintaining the magnetic nanoparticles properties unchanged. The preparation of SPIONs proceeded as follows:



For batch synthesis, 1.4 g of the iron precursor (FeSO<sub>4</sub> · 7H<sub>2</sub>O) were dissolved in 50 mL distilled water under continuous stirring for 30 min at 40 °C, until the solution color changed to yellow/green. An alkaline solution (20 mL of ammonium hydroxide) was then added slowly to the mixture to yield a dark green/black solution. The temperature was increased to 90 °C while stirring for additional 90 min, after which the mixture was cooled to room temperature. The precipitated SPIONs was separated from the supernatant using an external magnet, washed three times with distilled water (10 mL each) and rinsed with ethanol (5 mL). The SPIONs were left to dry at room temperature for 24 h or for 1 h by using a vacuum oven at 80 °C. For preparing GC-coated SPIONs, the particles were treated with three concentrations of GC (0.25 × 10<sup>-3</sup> mmol, 0.50 × 10<sup>-3</sup> mmol, and 0.75 × 10<sup>-3</sup> mmol dissolved in 100 mL of distilled water) under continuous mixing for 24 h.

### 2.3. Preparation of Progesterone-Loaded GC-Coated SPIONs

The progesterone loaded magnetic SPIONs coated with glycol chitosan were prepared with different progesterone initial loading of 5, 10, 15, 25, 50, and 75 mg. Each amount of progesterone was dissolved in 1 mL of acetone in a glass vial and added to 100 mg of SPION with vigorous mixing for 24 h. The progesterone loaded magnetic nanoparticles were washed with ethanol using the same procedure described above and then dried at room temperature.

### 2.4. Morphological, Structural and Magnetic Characterization of GC-Coated SPIONs

#### 2.4.1. Transmission Electron Microscopy (TEM)

Philips CM10 Transmission microscope was used with magnification range of 18× to 450,000×; resolution (objective lens): 0.5 nm/5.0 Å (point), 0.34 nm/3.4 Å (line); and accelerating voltage range of 40 kV to 100 kV. ImageJ software was used to analyze the particle size.

A total of 200 particle diameters for each sample were measured to obtain the particle size distribution, and three samples for each GC-coating concentration were analyzed.

#### 2.4.2. Scanning Electron Microscopy (SEM)

The surface morphology was examined using SEM (Hitachi High-Technologies GmbH, Germany). Before examining, the samples were placed on aluminum stubs then sputtered with gold and measured at an accelerating voltage of 20 kV coupled with energy dispersive X-ray spectroscopy (EDX) for elemental analysis.

#### 2.4.3. X-ray Diffraction (XRD) Analysis

The crystallite structure of Fe<sub>3</sub>O<sub>4</sub> nanoparticles was investigated using XRD powder analysis (MiniFlex-Rigaku, The Woodlands, TX) and the samples were exposed to radiation CuK $\alpha$ , 40 kV, 20 mA at a wavelength of 1.54 Å. The diffracting angle 2-theta covered from 15° to 65° with a 0.02° step size.<sup>21, 29, 30</sup>

#### 2.4.4. Fourier Transform Infrared (FTIR) Spectroscopy

A Bruker Vector 22 FTIR spectrometer controlled by OPUS 5.1 analytical software was used to obtain the FTIR spectra of the SPIONs samples in a powder state. The powder was scanned by an attenuated total reflectance (ATR) with resolution of 4 cm<sup>-1</sup> and total scans of 32. The samples were scanned between 4000–500 cm<sup>-1</sup>.

#### 2.4.5. Thermo-Gravimetric Analysis (TGA)

The weight percentage of GC attached to the SPIONs surface was analyzed by TGA with a range of 25 °C to 600 °C in air at a ramp rate of 10 °C min<sup>-1</sup>.

#### 2.4.6. Powder Magnetization

The magnetic properties were measured using a vibrating sample magnetometer (7407 VSM, Lake Shore cryotronics, Westerville, OH). The magnetic properties of SPIONs samples were studied at moment measure range of 10<sup>-7</sup> to 10<sup>3</sup> emu, 0.05% full scale with field accuracy. All the magnetization measurements were carried out at room temperature under a maximum field of 10 kOe.

### 2.5. Progesterone Loading and Encapsulation Efficiency

Drug loading is defined as the amount of drug encapsulated inside the nanoparticles per unit mass.<sup>21</sup> SPIONs were loaded with various amounts of progesterone, which was predetermined according to its solubility in aqueous solution (5, 10, 15, 25, 50, and 75 mg). The concentration of encapsulated progesterone was determined by dissolving 10 mg of nanoparticles in absolute ethanol. After 24 h of stirring, the supernatant was analyzed for the progesterone concentration using UV spectrophotometry. The ratio of the amount of progesterone encapsulated in the SPIONs to the total amount of drug loaded is the

**Table I.** Effect of GC coating concentration on the measured particle size of bare and GC-coated SPIONs using TEM images and the calculated values based on XRD.

Sample code	GC concentration (mmol)	Particle size (nm, estimated from the XRD pattern)	Particle size (nm, measured using TEM)	GC coating thickness (nm, measured using TEM)
Uncoated Fe <sub>3</sub> O <sub>4</sub>	0	10.31	8.76 ± 2.00	–
Fe <sub>3</sub> O <sub>4</sub> -GC 1	0.25 × 10 <sup>-3</sup>	12.71	11.87 ± 3.20	1.56 ± 0.60
Fe <sub>3</sub> O <sub>4</sub> -GC 2	0.50 × 10 <sup>-3</sup>	15.68	12.20 ± 2.61	1.72 ± 0.31
Fe <sub>3</sub> O <sub>4</sub> -GC 3	0.75 × 10 <sup>-3</sup>	18.41	20.40 ± 3.24	5.82 ± 0.62

encapsulation efficiency (Table I). Each measurement was repeated in triplicate. Equations (4) and (5) were used in the calculation.

$$\begin{aligned} & \% \text{ encapsulation efficiency} \\ & = \left[ \frac{\text{amount of drug encapsulated}}{\text{total amount of initial loaded drug}} \right] \times 100 \quad (4) \end{aligned}$$

$$\begin{aligned} & \% \text{ Drug loading} \\ & = \left[ \frac{\text{Weight of drug encapsulated}}{\text{Weight of dry nanoparticles}} \right] \times 100 \quad (5) \end{aligned}$$

### 2.6. In-Vitro Release Study of GC-Coated SPIONs

Progesterone release was carried out in a dialysis bag (Pur-A-Lyzer Mega 12000). The dialysis bag insured that diffusion occurred only for drug molecules without the passage of any SPIONs. GC-coated SPIONs at the different coating concentrations loaded with 5 mg progesterone were placed in 10 mL of the release media in the inner tube of the dialyzer. Progesterone was freely soluble in the media with an addition of 0.5 mL of acetone and 0.1% of Tween 20. The dialyzer was placed into a 60 mL beaker containing the release media. Two release media were used: distilled water or phosphate-buffered saline (PBS) to compare the release at different pH values, 6.5 and 7.4, respectively. The setup was placed in an incubating shaker set at 37 °C and 300 rpm, in order to maintain homogeneity at the membrane/outer media interface. The progesterone diffusion was measured by sampling 5 mL of the outer solution at predetermined time intervals. Fresh solution of distilled water or PBS solution was replaced in the breaker. The released progesterone was measured at wavelength of 450 nm.

### 2.7. In-Vitro Cytotoxicity Study of GC-Coated SPIONs

Time-course and dose-course cytotoxicity of the progesterone-loaded GC-SPIONs were evaluated using C3H10T1/2 mouse mesenchymal progenitor cell line, where the metabolic cell activity was measured by MTT assay following the manufacturer's protocol (Vybrant®, Invitrogen, Burlington, ON). In the dose-course study,

cells were pre-cultured for 24 h after seeding at a density of 8,000 cells/well in 96-well plates. Afterwards, C3H10T1/2 were treated with various concentrations of progesterone-loaded nanoparticles (25, 50, 75, and 100  $\mu\text{g}/\text{mL}$ ) with various coating concentrations of GC in the presence of 10% FBS. After 48 h of incubation at 37 °C, MTT solution (5 mg/mL in PBS) was added to each well and the absorbance was measured at 570 nm using a micro-plate reader (UVM 340, Montreal Biotech Inc., Dorval, QC). The same procedure was used in the time-course study; however, 50  $\mu\text{g}/\text{mL}$  progesterone concentration was tested and cells were treated with progesterone-loaded SPIONs with different GC coating concentrations and without GC coating (as a control). Then, MTT absorbance values were measured following 48 h and 96 h of culture.

### 2.8. Statistical Analysis

Where applicable, experimental data is presented as mean  $\pm$  standard deviation (SD) and was analyzed statistically by one-way analysis of variance and the level of significance was determined at  $p < 0.05$ .

## 3. RESULTS AND DISCUSSION

### 3.1. The Effect of GC Coating on the Morphological and Structural Properties of SPIONs

Figures 1(A) and (B) respectively show representative TEM and SEM images of uncoated and GC-coated SPIONs with varied GC concentrations presented in Table I. The corresponding histogram of particle size distribution for uncoated and GC-coated SPIONs (GC concentration of  $0.5 \times 10^3$  mmol), determined by ImageJ analysis is shown in Figure 1(C). Spherical-like agglomerated SPIONs were clearly observed in Figure 1(A) (1–4), due to the magnetic dipolar forces and van der Waals forces between the nanoparticles. As shown, GC-coated SPIONs maintained nearly spherical shape with wider separation of particles compared to uncoated particles (Fig. 1(A)). This suggests that the forces between the particles had likely decreased due to the surface modification with GC coating. In addition, individual particle size had increased because of the GC coating of the SPIONs, starting with particle size of  $8.76 \pm 2.0$  nm for uncoated SPIONs up to 20.40 to  $\pm 3.24$  nm for highest tested GC-coating concentration (Table I). The increase in particle

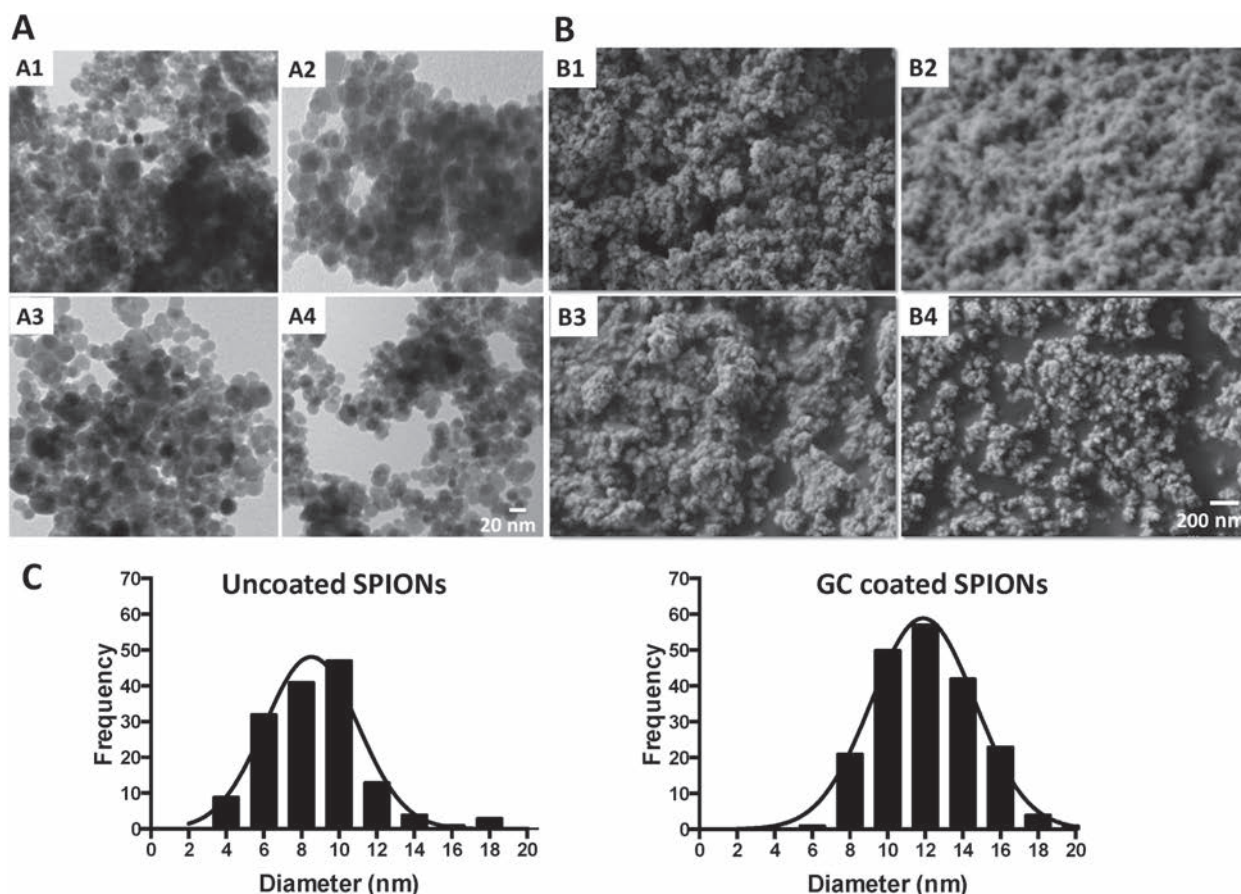


**Fig. 1.** Size and morphology of SPIONs. (A) Transmission electron micrographs illustrating the effect of polymeric GC coating on bare SPIONs: (A1) uncoated SPIONs, (A2) Fe<sub>3</sub>O<sub>4</sub>-GC 1, (A3) Fe<sub>3</sub>O<sub>4</sub>-GC 2, (A4) Fe<sub>3</sub>O<sub>4</sub>-GC 3, (B) scanning electron micrographs for different magnetic nanoaggregates showing the effect of polymeric composition of GC on their morphology: (B1) uncoated SPIONs, (B2) Fe<sub>3</sub>O<sub>4</sub>-GC 1, (B3) Fe<sub>3</sub>O<sub>4</sub>-GC 2, (B4) Fe<sub>3</sub>O<sub>4</sub>-GC 3, (C) histogram of particle size distribution for uncoated and GC-coated SPIONs.

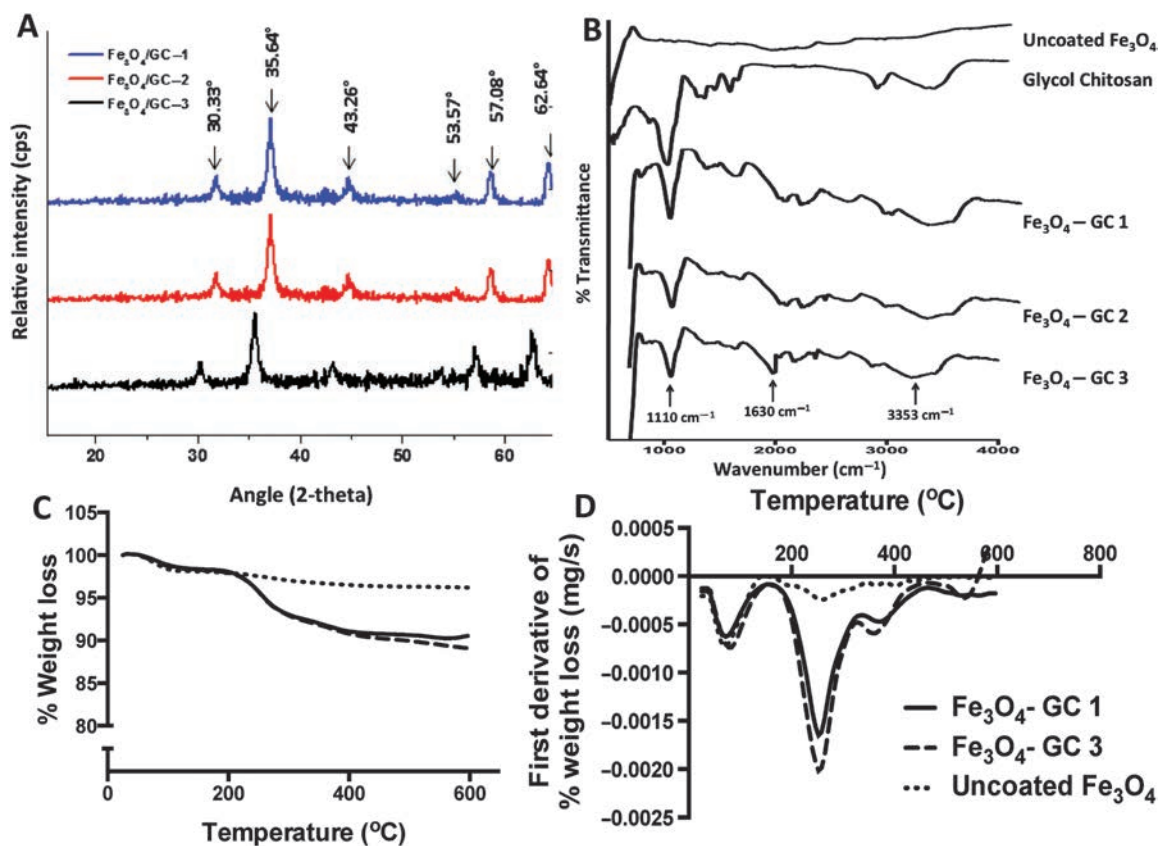


**Fig. 2.** Characterization techniques of SPIONs. (A) X-ray diffraction (XRD) pattern demonstrating the effect of GC coating on the crystalline structure of SPIONs, (B) FTIR spectra of uncoated SPIONs, pure glycol chitosan (GC), and GC-coated magnetic nanoparticles, (C) TGA profile of GC-coated magnetic nanoparticles, (D) first derivative of % weight loss for uncoated and GC-coated Fe<sub>3</sub>O<sub>4</sub> nanoparticles.

size may indicate that GC was evenly surrounding the core SPIONs in a core/shell structure. In Figure 1(C), uncoated SPIONs tend to show a particle size distribution skewed to the right, while GC-coated SPIONs showed a normal distribution with a narrower distribution range suggesting a lower degree of aggregation with GC coating in comparison to bare SPIONs.

Spherical drug delivery vehicles are much more favored due to their ability to be taken up more readily by the cells than shapes with higher length-to-width ratio, which can enrich the possibilities in terms of controlled release rate, pharmacokinetics, and delivery performance.<sup>31,32</sup> Uncoated SPIONs tended to cluster; however, the clustering decreased as the GC coating was introduced and it further decreased as thicker GC coating was used without affecting the particle morphology. In fact, it is apparent that in the case of Fe<sub>3</sub>O<sub>4</sub>-GC 3 (Fig. 1(B4)), the nanoparticles were much more separated and homogeneously distributed.

XRD measurements were conducted to verify the formation of crystalline magnetite and that the polymer coating did not affect the magnetite crystalline phase. In Figure 2(A), iron oxide nanoparticles show sharp prominent peaks at 30.5 (220), 35.84 (311), 43.46 (400), 53.90 (422), 57.38 (511) and 62.90 (440) with 311 peak having

the highest intensity.<sup>33,34</sup> These peaks with similar intensities and with the corresponding angles were present in all of the tested samples suggesting that the prepared SPIONs by alkaline precipitation corresponded to the pure phase of Fe<sub>3</sub>O<sub>4</sub> and that the preparation was feasible. It was found that the addition of different concentrations of GC coating did not alter the XRD spectrum, since the same peaks were present indicating that the spinel structure of Fe<sub>3</sub>O<sub>4</sub> was retained.<sup>34</sup> The width of the diffraction peak is related to the size of the crystalline particles whereby narrow diffraction peak corresponded to large particle sizes.<sup>29</sup> The average particle size of SPIONs (*D*) can be calculated using Scherrer's equation (Eq. (6)).

$$D = \frac{K\lambda}{(\beta \cos \theta)} \quad (6)$$

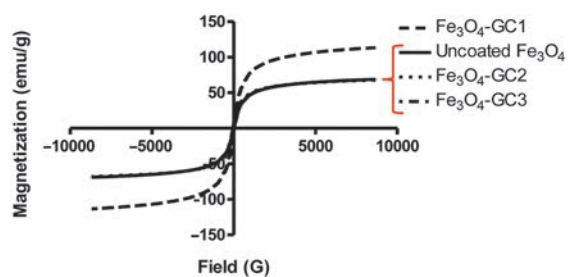
Where, *K* is a constant,  $\lambda$  is the X-ray wavelength,  $\beta$  is the peak width of half-maximum and  $\theta$  is the Bragg diffraction angle.<sup>35</sup> The particle size of SPIONs obtained from XRD increased with polymer coating, which was in good agreement with TEM data (Table I). The FTIR spectra in Figure 2(B) showed the presence of GC coating on the Fe<sub>3</sub>O<sub>4</sub> nanoparticles. The band at 3353 cm<sup>-1</sup> is attributed to the stretching vibration of O-H and N-H while the peak at 2925 cm<sup>-1</sup> is the C-H stretching. The absorption band at

around 1630 cm<sup>-1</sup> in the pure GC and the coated samples corresponded to the amide bond of the deacetylated section of GC; whereas, this peak was absent in the bare SPIONs. The glycosidic linkage (ether bond) and C–N vibrations appeared at 1110 and 1062 cm<sup>-1</sup>, respectively. The peak at 586 cm<sup>-1</sup> which appeared only in the coated samples is the Fe–O stretching vibration of Fe<sub>3</sub>O<sub>4</sub>.<sup>36</sup> This shift of the amide bond from 1677 to 1630 cm<sup>-1</sup> in GC-coated Fe<sub>3</sub>O<sub>4</sub> NPs indicated the interaction between GC and SPIONs.

### 3.2. The Effect of GC Coating on Thermal and Magnetic Properties of SPIONs

TGA measurements were conducted to confirm the GC coating of the SPIONs and to determine the amount of GC coating (Figs. 2(C and D)). It is shown that the percentage residual weight for uncoated, Fe<sub>3</sub>O<sub>4</sub>-GC 1, and Fe<sub>3</sub>O<sub>4</sub>-GC 3 were 96.02%, 89.17%, and 90.46%, respectively. This observed weight loss for the GC coated SPIONs is due to the decomposition of the GC coating layer. The TGA results clearly showed that the coated nanoparticles were significantly different from the uncoated SPIONs, and both Fe<sub>3</sub>O<sub>4</sub>-GC 1 and Fe<sub>3</sub>O<sub>4</sub>-GC 3 displayed similar weight loss profile below 400 °C. The initial stage of weight loss was around 2% for all samples within the first 200 °C most likely related to the removal of adsorbed moisture. The weight loss observed for the uncoated SPIONs at around 350 °C is attributed to the decomposition of amorphous iron hydroxides as reported in the literature.<sup>37</sup>

Powder magnetization was studied to determine how the magnetic properties were affected after surface modification via GC surface coating. Vibrating sample magnetometer (VSM) was used to measure the magnetic properties for uncoated and the three GC-coated SPIONs. Figure 3 shows a typical magnetization pattern for uncoated and GC-coated SPIONs. A superparamagnetic property was demonstrated, where the hysteresis loops for all samples



Sample Code	Magnetization (emu/g)	Retentivity (emu/g)	Coercivity (G)
Uncoated Fe <sub>3</sub> O <sub>4</sub>	68.98	2.54	1.56
Fe <sub>3</sub> O <sub>4</sub> -GC1	113.39	7.56	4.84
Fe <sub>3</sub> O <sub>4</sub> -GC2	67.88	0.19	0.95
Fe <sub>3</sub> O <sub>4</sub> -GC3	68.67	4.97	4.62

**Fig. 3.** Hysteresis curves at room temperature of bare and GC coated SPIONs illustrating the effect of GC coating on the magnetization and the superparamagnetic property of magnetic nanoaggregates.

indicated a single-domain magnetic nanoparticle. Retentivity is a measure of the remaining magnetization after the driving field drops to zero, while coercivity is the measure of the reverse field needed to drive the magnetization to zero after it had reached saturation. When these two values approach zero, it indicates a maximum superparamagnetic property. This is a standard property for maghemite and magnetite with diameters between 10 and 20 nm.<sup>38,39</sup> This attractive feature allows them to be recovered from one site and directed to other sites for their reuse in drug delivery applications after the payload is done as they have the ability to demagnetize once the external magnetic field is removed.<sup>40</sup> Fe<sub>3</sub>O<sub>4</sub>-GC 2 showed a particular superparamagnetic characteristic surpassing the uncoated SPIONs by showing lower retentivity and coercivity values. Fe<sub>3</sub>O<sub>4</sub>-GC 1 and Fe<sub>3</sub>O<sub>4</sub>-GC 3 had higher retentivity and coercivity compared to Fe<sub>3</sub>O<sub>4</sub>-GC 2. Since magnetic particles having less than 20 Oe coercivity fall within the superparamagnetic family,<sup>41</sup> all GC coated samples were superparamagnetic. Within the GC coated SPIONs, the decrease in superparamagnetic property for Fe<sub>3</sub>O<sub>4</sub>-GC 1 and Fe<sub>3</sub>O<sub>4</sub>-GC 3 may be due to the increase in particle size because of the thicker GC layer incorporated as stated in Table I. This is also evident from the increase of retentivity compared to the uncoated SPIONs. The presence of GC on the particle surface decreased their uniformity due to the reduction in the surface moment, which sequentially decreased the magnetic moment of these particles. The measured saturation magnetization values for Fe<sub>3</sub>O<sub>4</sub>-GC 2 and Fe<sub>3</sub>O<sub>4</sub>-GC 3 were close to the uncoated SPIONs value, which in turn, were similar to reported values for other coated systems.<sup>42,43</sup> Interestingly, Fe<sub>3</sub>O<sub>4</sub>-GC 1 showed significant increase in magnetic saturation that needs further investigation. Altogether, the prepared GC-coated SPIONs could provide potential application in targeted delivery with ease of post-delivery separation due to their inherent magnetic properties.

### 3.3. Progesterone Loading and Its *In-Vitro* Release Study of from GC-Coated SPIONs

As shown in Table II, changing the coating concentration of glycol chitosan in the compositions significantly increased the drug encapsulation efficiency. In fact, the % encapsulation efficiency of Fe<sub>3</sub>O<sub>4</sub>-GC 3 had almost doubled compared to uncoated Fe<sub>3</sub>O<sub>4</sub> nanoparticles (from 34.02% ± 3.54% to 63.54% ± 3.4.65%). The % encapsulation efficiency and % drug loading decreased when GC concentrations higher than 0.75 × 10<sup>-3</sup> mmol were used (data not shown). This may be due to the saturation of the GC coating that prevented progesterone from penetrating through the GC network. Moreover, the progesterone-loading increased with increasing the surface coating (Table II). Glycol chitosan is a self-assembled polymeric amphiphile, where the hydrophobic moieties are facing towards the core, and the hydrophilic moieties are facing towards the solution.<sup>44</sup> For this reason, GC is

**Table II.** Percentage encapsulation efficiency, percentage drug loading and release rate constants at different pH for coated and uncoated SPIONs.

Sample code	Progesterone		Release rate constant (pH 6.5) ( <i>k</i> , day <sup>-1</sup> )	Release rate constant (pH 7.4) ( <i>k</i> , day <sup>-1</sup> )
	encapsulation efficiency (%)	Progesterone loading (%)		
Uncoated Fe <sub>3</sub> O <sub>4</sub>	34.02 ± 3.54	12.40 ± 0.35	–	–
Fe <sub>3</sub> O <sub>4</sub> -GC 1	35.49 ± 1.84	16.51 ± 2.89	11.2615 ± 0.32	–
Fe <sub>3</sub> O <sub>4</sub> -GC 2	46.82 ± 5.78	31.76 ± 6.21	9.0170 ± 0.58	–
Fe <sub>3</sub> O <sub>4</sub> -GC 3	63.54 ± 4.65	38.23 ± 5.7	9.0170 ± 0.58	14.0973 ± 1.15

freely soluble in water at a wide pH range.<sup>45</sup> When GC encounters the hydrophobic progesterone, they are likely to form weaker interactions such as hydrogen bonding, hydrophilic/hydrophobic and electrostatic interactions.<sup>45, 46</sup> These bonds are expected to be formed at the internal surface of the GC shell. Hence, progesterone will be encapsulated into the SPION core and GC shell. The more binding

sites are available, the higher the chance for progesterone molecules to attach to GC. This suggests the increased loading % of progesterone with higher concentrations of GC coating.

The release profiles of progesterone from Fe<sub>3</sub>O<sub>4</sub>-GC SPIONs at pH 6.5 are presented in Figure 4(A). For all surface coated magnetic nanoparticles, the initial burst release was observed within the first 3 h with 5% maximum cumulative progesterone released. This strongly corresponds to the release of drug adsorbed to the surface of the nanoparticles. GC-coated Fe<sub>3</sub>O<sub>4</sub> SPIONs exhibited sustained release 64.82%, 30.00%, and 25.50% for Fe<sub>3</sub>O<sub>4</sub>-GC 1, Fe<sub>3</sub>O<sub>4</sub>-GC 2 and Fe<sub>3</sub>O<sub>4</sub>-GC 3, respectively over 15 days and release rate reached equilibrium state at Day 16. In nanoparticle drug delivery systems, polymer degradation plays an important role in the release of the drug. Since GC is soluble in water, it tends to degrade faster in hydrophilic solutions in a shear thinning behaviour, compared to other hydrophobic polymers. Also, the type of bonds and cross-linking of polymer to drug/nanoparticles

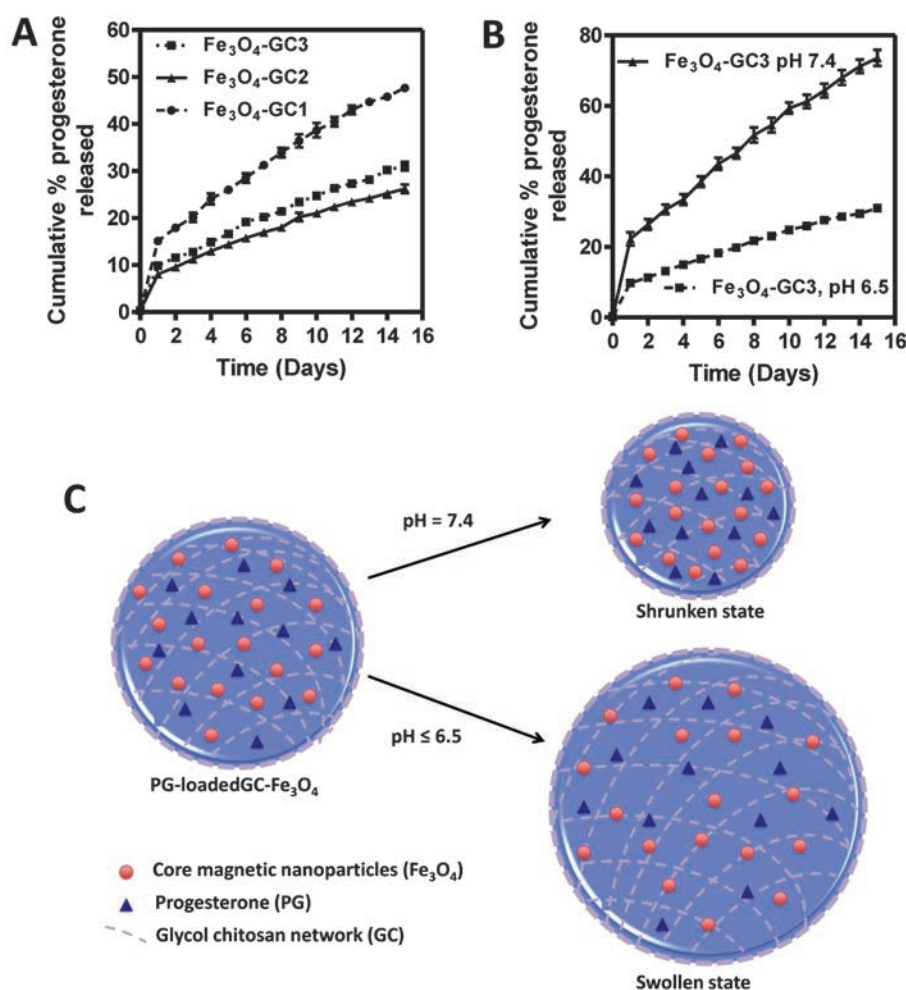


**Fig. 4.** Release profiles of progesterone from variable GC coated SPION formulations: (A) The effect of increasing GC surface coating on Fe<sub>3</sub>O<sub>4</sub> at 5 mg progesterone initial loading, (B) the effect of pH value on the release profile of the highest concentration of GC coated SPIONs (Fe<sub>3</sub>O<sub>4</sub>-GC 3). (C) Proposed pH-responsive release mechanism of Fe<sub>3</sub>O<sub>4</sub>-glycol chitosan hybrid magnetic nanoparticles.

greatly influence release rates.<sup>47</sup> Moreover, the combination of both drug diffusion and polymer degradation can play an important role in influencing the release rates of progesterone from GC-coated Fe<sub>3</sub>O<sub>4</sub> SPIONs.<sup>48</sup>

### 3.3.1. The Effect of pH on Progesterone Release Profile from GC-Coated SPIONs

The release of progesterone from Fe<sub>3</sub>O<sub>4</sub>-GC 3 was investigated at two different pH release media (6.5 and 7.4). The maximum cumulative released amount of progesterone (Day 15) was 72.02% at pH 7.4, while the cumulative released amount decreased to 30.00% at pH 6.5. However, similar release trends were observed for both, where the samples exhibited an initial fast burst release followed by relatively slower release till equilibrium was reached (Fig. 4(B)). This could be explained by the swelling properties of glycol chitosan with the change in the pH of the release medium.<sup>49</sup> At relatively lower pH value (pH 6.5), the GC shell is protonated and swelled to block the pores in the Fe<sub>3</sub>O<sub>4</sub>-GC network structure; which explains the lower rate of drug permeation. On the other hand, the enhanced rate of drug release at pH value 7.4 was attributed to GC shrinkage, which was expected to result in less pore blockage in the Fe<sub>3</sub>O<sub>4</sub>-GC network structure (Fig. 4(C)). Moreover, the permeation of progesterone through the GC shell itself increased due to the protonation of the free amino group at lower pH value. The pH change resulted in uncoiled and more elongated GC networks. In addition, the pH reduction of the release medium resulted in an increase in the internal osmotic pressure and mutual repulsion of the charged amino groups, which induced the uncoiling of the GC networks.<sup>50</sup>

As mentioned above, the overall release rate of progesterone is dependent on its permeation through the pores between GC and Fe<sub>3</sub>O<sub>4</sub>, and the permeation of progesterone through the GC shell itself. The overall release rate increase at pH 7.4 may be explained by faster permeation of progesterone through the pores between GC and Fe<sub>3</sub>O<sub>4</sub> than through the GC shell itself.

### 3.3.2. Study of the Kinetics of Progesterone Release from GC-Coated SPIONs Though Various Mathematical Models

Mathematical investigation of progesterone release process was conducted by fitting the experimental data to

various release kinetic models, namely: Baker-Lonsdale, Korsmeyer-Peppas, Hixon and crowell, Higuchi equation, and first-order equation.<sup>51</sup> From Table III, it can be seen that Baker-Lonsdale and Korsmeyer-Peppas models best described the progesterone release from GC-coated Fe<sub>3</sub>O<sub>4</sub> nanoparticles, as the correlation coefficient was greater than 0.969 under the three different GC-coating concentrations. The drug release was mainly based on diffusion mechanism as suggested by Korsmeyer-Peppas model. More specifically, for Fe<sub>3</sub>O<sub>4</sub>-GC 1 the model indicated an anomalous diffusion ( $0.43 < n < 1.0$ ) while Fe<sub>3</sub>O<sub>4</sub>-GC 2 and Fe<sub>3</sub>O<sub>4</sub>-GC 3 exhibited a Fickian diffusion with  $n = 0.43$  for spherical particles.<sup>52</sup> Baker-Lonsdale model proposes that the drug release was carried out through spherical non-homogenous polymeric matrix across the capillaries and fractures in the system.<sup>53</sup> Overall, it can be concluded that the release mechanism was a combination of drug diffusion from magnetic core as well as drug release due to the disintegration and deterioration of the polymeric matrix.

### 3.4. Cytotoxicity Study of Progesterone-Loaded GC-Coated SPIONs

Figure 5(A) shows the dose-course metabolic activity of C3H10T1/2 cells treated with various concentrations of progesterone-loaded nanoparticles (25, 50, 75, and 100 µg/mL) with various coating concentrations of GC as determined by MTT assay. The uncoated nanoparticles did not show any significant difference in metabolic activity in all concentrations except for 100 µg/mL of progesterone-loaded nanoparticles. For coated nanoparticles, only 25 µg/mL demonstrated insignificant decrease, whereas 50, 75 and 100 µg/mL had a significantly decreased metabolic activity in comparison to the untreated control but not significantly different from the bare nanoparticles. This suggests that the uncoated and unloaded SPIONs did not cause any cytotoxic effects to the cells. However, when the GC-coated Fe<sub>3</sub>O<sub>4</sub> nanoparticles are loaded with progesterone, it affected the metabolic activity of the cells at higher concentrations. Fe<sub>3</sub>O<sub>4</sub>-GC 1 showed the highest drop in metabolic activity compared to Fe<sub>3</sub>O<sub>4</sub>-GC 2 and Fe<sub>3</sub>O<sub>4</sub>-GC 3, this can be explained by the fast in-vitro release of progesterone in Fe<sub>3</sub>O<sub>4</sub>-GC 1 compared to the other coated samples within the first 24 hours (Fig. 4(A), Table II). The significant decrease in metabolic activity

**Table III.** Correlation coefficients values of progesterone cumulative release curves from GC-coated Fe<sub>3</sub>O<sub>4</sub> NPs fitted kinetic models fitted to different kinetic models.

Sample code	Baker-Lonsdale model		Korsmeyer-Peppas model		Higuchi model		Hixon and Crowell model		First-order model	
	R <sup>2</sup>	K	R <sup>2</sup>	K	R <sup>2</sup>	K	R <sup>2</sup>	K	R <sup>2</sup>	K
Fe <sub>3</sub> O <sub>4</sub> -GC 1	0.994	0.003	0.997	11.262	0.997	11.818	0.936	0.0145	0.948	0.0477
Fe <sub>3</sub> O <sub>4</sub> -GC 2	0.969	0.011	0.974	9.017	0.969	7.622	0.850	0.009	0.860	0.028
Fe <sub>3</sub> O <sub>4</sub> -GC 3	0.969	0.014	0.9743	9.576	0.9688	7.615	0.8192	0.006	0.8709	0.038

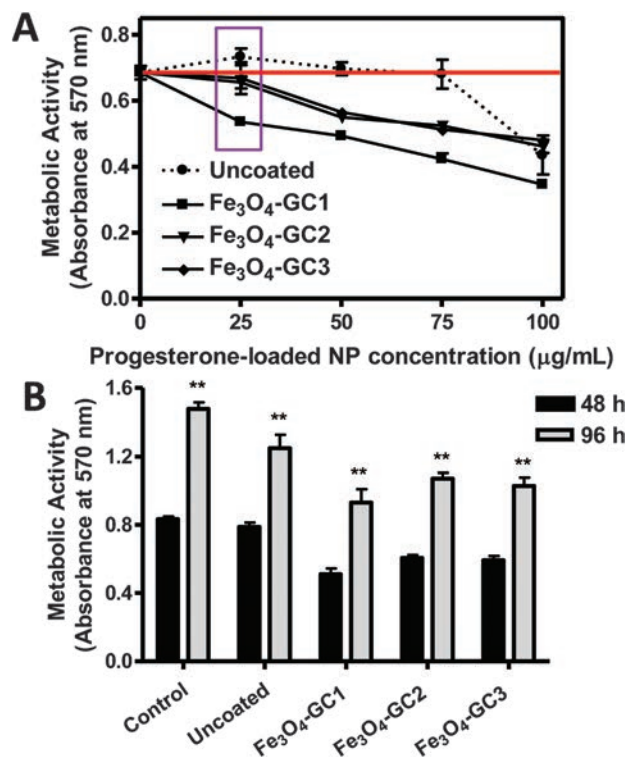


**Fig. 5.** Cytotoxicity study for the uncoated and GC-coated SPIONs using C3H10T1/2 cells determined by MTT assay illustrating (A) the dose effect of progesterone loaded SPIONs for 48 h and (B) the culture time effect. \*\* indicates ( $p < 0.01$ ).

above 25 µg/mL of progesterone-loaded GC-coated Fe<sub>3</sub>O<sub>4</sub> nanoparticles was probably due to the higher percentage of progesterone loading in the case of GC-coated nanoparticles versus the uncoated particles. By decreasing the progesterone-loaded GC-coated Fe<sub>3</sub>O<sub>4</sub> concentration in the culture media, the level of cytotoxicity decreased. Also, the time-course study (Fig. 5(B)) demonstrated the ability of the 10T1/2 cells to grow and function under the treatment with progesterone-loaded GC-SPIONs (25 µg/mL). Cells were able to grow in a time-dependent manner for 96 h demonstrating the biocompatibility of the GC-SPIONs *in-vitro*. Overall, the cytotoxicity study results had shown that the prepared GC-SPIONs are well tolerated by C3H10T1/2 cells.

#### 4. CONCLUSIONS

Polymeric-metallic hybrid nanoparticles were prepared with different compositions of glycol chitosan. The *in-vitro* release study of progesterone-loaded Fe<sub>3</sub>O<sub>4</sub>-GC NPs in PBS demonstrated that slight changes in the pH of the release media yielded an increase in the rate of drug diffusion, due to the swelling behaviour of glycol chitosan at pH 6.5 and shrinking at pH 7.4. In addition, testing the metabolic cell activity of 10T1/2 cells under the treatment with unloaded and progesterone-loaded Fe<sub>3</sub>O<sub>4</sub>-GC NPs showed that the magnetic nanoparticles had good

biocompatibility. The suggested dual stimuli-responsive nanoparticles can be a promising candidate for targeted and controlled drug delivery, owing to the magnetic properties of their magnetite core and the pH-responsive properties of their glycol chitosan shell.

**Acknowledgment:** The authors are grateful for the Natural Sciences and Engineering Research Council of Canada for the financial support.

#### References and Notes

- Z. Karimi, L. Karimi, and H. Shokrollahi, Nano-magnetic particles used in biomedicine: Core and coating materials. *Mater. Sci. Eng. C* 33, 2465 (2013).
- A. Tomitaka, T. Koshi, S. Hatsugai, T. Yamada, and Y. Takemura, Magnetic characterization of surface-coated magnetic nanoparticles for biomedical application. *Proc. 12th Int. Conf. Magn. Fluid* (2011), Vol. 323, pp. 1398–403.
- A. Jhaveri, P. Deshpande, and V. Torchilin, Stimuli-sensitive nanopreparations for combination cancer therapy. *30th Anniv. Spec. Issue* 190, 352 (2014).
- Y. Gao, J. Xie, H. Chen, S. Gu, R. Zhao, J. Shao, and L. Jia, Nanotechnology-based intelligent drug design for cancer metastasis treatment. *Biotechnol. Nanomedicine* 32, 761 (2014).
- A. Ito, M. Shinkai, H. Honda, and T. Kobayashi, Medical application of functionalized magnetic nanoparticles. *J. Biosci. Bioeng.* 100, 1 (2005).
- N. Kamaly, Z. Xiao, P. M. Valencia, A. F. Radovic-Moreno, and O. C. Farokhzad, Targeted polymeric therapeutic nanoparticles: Design, development and clinical translation. *Chem. Soc. Rev.* 41, 2971 (2012).
- A. K. Gupta and M. Gupta, Synthesis and surface engineering of iron oxide nanoparticles for biomedical applications. *Biomaterials* 26, 3995 (2005).
- A. Singh and S. K. Sahoo, Magnetic nanoparticles: A novel platform for cancer theranostics. *Drug Discov. Today* 19, 474 (2014).
- S. Laurent, D. Forge, M. Port, A. Roch, C. Robic, L. V. Elst, and R. N. Muller, Magnetic iron oxide nanoparticles: Synthesis, stabilization, vectorization, physicochemical characterizations, and biological applications. *Chem. Rev.* 108, 2064 (2008).
- P. Mulvaney, L. M. Liz-Marzan, M. Giersig, and T. Ung, Silica encapsulation of quantum dots and metal clusters. *J. Mater. Chem.* 10, 1259 (2000).
- A. J. Wagstaff, S. D. Brown, M. R. Holden, G. E. Craig, J. A. Plumb, R. E. Brown, N. Schreiterb, W. Chrzanowskia, and N. J. Wheate, Cisplatin drug delivery using gold-coated iron oxide nanoparticles for enhanced tumour targeting with external magnetic fields. *Spec. Issue Met. Med.* 393, 328 (2012).
- J. Hradil, A. Pisarev, M. Babič, and D. Horák, Dextran-modified iron oxide nanoparticles. *Magn. Part Syst.* 5, 162 (2007).
- M. R. Phadatare, V. M. Khot, A. B. Salunkhe, N. D. Thorat, and S. H. Pawar, Studies on polyethylene glycol coating on NiFe<sub>2</sub>O<sub>4</sub> nanoparticles for biomedical applications. *J. Magn. Magn. Mater.* 324, 770 (2012).
- A. M. G. C. Dias, A. Hussain, A. S. Marcos, and A. C. A. Roque, A biotechnological perspective on the application of iron oxide magnetic colloids modified with polysaccharides. *Biotechnol. Adv.* 29, 142 (2011).
- G. Unsoy, S. Yalcin, R. Khodadust, P. Mutlu, O. Onguru, and U. Gunduz, Chitosan magnetic nanoparticles for pH responsive Bortezomib release in cancer therapy. *Biomed. Pharmacother.* 68, 641 (2014).
- J.-P. Chen, P.-C. Yang, Y.-H. Ma, and T. Wu, Characterization of chitosan magnetic nanoparticles for *in situ* delivery of tissue plasminogen activator. *Carbohydr. Polym.* 84, 364 (2011).

17. J. Bulte, M. De Cuyper, Magnetoliposomes as contrast agents. *Methods Enzymol.* 373, 175 (2003).
18. Inc IB& M, Magnetic Nanomaterials, Book by Challa S. S. R. Kumar (Hardcover) chapters.indigo.ca [Internet], indigo.ca. [cited 2016 August], Available from: <https://www.chapters.indigo.ca/en-ca/books/magnetic-nanomaterials/9783527321544-item.html>.
19. Markovic, Mutschler, Wöllner, and Gauglitz, Application of surface acoustic waves for optimisation of biocompatibility of carboxymethylated dextran surfaces. *ResearchGate* 201, 1282 (2006).
20. S. C. McBain, H. H. P. Yiu, and J. Dobson, Magnetic nanoparticles for gene and drug delivery. *Int. J. Nanomedicine* 3, 169 (2008).
21. D. Ragab, S. Rohani, and S. Consta, Controlled release of 5-fluorouracil and progesterone from magnetic nanoaggregate. *Int. J. Nanomedicine* 7, 3167 (2012).
22. L. A. Barros, S. Tufik, and M. L. Andersen, The role of progesterone in memory: An overview of three decades. *Neurosci. Biobehav. Rev.* 49, 193 (2015).
23. S. N. Kaore, D. K. Langade, V. K. Yadav, P. Sharma, V. R. Thawani, and R. Sharma, Novel actions of progesterone: What we know today and what will be the scenario in the future? *J. Pharm Pharmacol.* 64, 1040 (2012).
24. M. L. Andersen and S. Tufik, Does male sexual behavior require progesterone? *Brain Res. Rev.* 51, 136 (2006).
25. K. C. Un, Y. C. Wang, W. Wu, and G. K. K. Leung, Systemic progesterone for modulating electrocautery-induced secondary brain injury. *J. Clin. Neurosci.* 20, 1329 (2013).
26. D. Si, H. Wang, Q. Wang, C. Zhang, J. Sun, Z. Wang, Z. Zhang, and Y. Zhang, Progesterone treatment improves cognitive outcome following experimental traumatic brain injury in rats. *Neurosci. Lett.* 553, 18 (2013).
27. F. Sonvico, S. Mornet, S. Vasseur, C. Dubernet, D. Jaillard, J. Degrouard, J. Hoebeke, E. Duguet, P. Colombo, and P. Couvreur, Folate-conjugated iron oxide nanoparticles for solid tumor targeting as potential specific magnetic hyperthermia mediators: Synthesis, physicochemical characterization, and *in vitro* experiments. *Bioconjug. Chem.* 16, 1181 (2005).
28. US Department of Health and Human Service, Cancer nanotechnology: Going small for big advances—Using nanotechnology to advance cancer diagnosis, prevention and treatment, National Institute of Health and National Cancer Institute (2004).
29. S. Hribernik, M. Sfiligoj-Smole, M. Bele, S. Gyergyek, J. Jamnik, and K. Stana-Kleinschek, Synthesis of magnetic iron oxide particles: Development of an *in situ* coating procedure for fibrous materials. *Colloids Surf. Physicochem. Eng. Asp.* 400, 58 (2012).
30. F. Jiang, X. Li, Y. Zhu, and Z. Tang, Synthesis and magnetic characterizations of uniform iron oxide nanoparticles. *Phys. B Condens. Matter.* 443, 1 (2014).
31. A. Hadjitheodorou and G. Kalosakas, Analytical and numerical study of diffusion-controlled drug release from composite spherical matrices. *Mater. Sci. Eng. C* 42, 681 (2014).
32. Y. Geng, D. E. Discher, T. Minko, S. Cai, P. Dalhaimer, M. Tewari, T. Minko, and D. E. Discher, Shape effects of filaments versus spherical particles in flow and drug delivery. *Nat. Nanotechnol.* 2, 249 (2007).
33. C.-C. Lin and J.-M. Ho, Structural analysis and catalytic activity of Fe<sub>3</sub>O<sub>4</sub> nanoparticles prepared by a facile co-precipitation method in a rotating packed bed. *Ceram Int.* 40, 10275 (2014).
34. S. Zhou, Y. Li, F. Cui, M. Jia, X. Yang, Y. Wang, L. Xie, Q. Zhang, and Z. Hou, Development of multifunctional folate-poly(ethylene glycol)-chitosan-coated Fe<sub>3</sub>O<sub>4</sub> nanoparticles for biomedical applications. *Macromol. Res.* 22, 58 (2014).
35. A. W. Burton, K. Ong, T. Rea, and I. Y. Chan, On the estimation of average crystallite size of zeolites from the Scherrer equation: A critical evaluation of its application to zeolites with one-dimensional pore systems. *Microporous Mesoporous Mater.* 117, 75 (2009).
36. R. Kumar, B. S. Inbaraj, and B. H. Chen, Surface modification of superparamagnetic iron nanoparticles with calcium salt of poly( $\gamma$ -glutamic acid) as coating material. *Mater. Res. Bull.* 45, 1603 (2010).
37. Baskaran Stephen Inbaraj and T.-Y. Tsai, and B., Synthesis, characterization and antibacterial activity of superparamagnetic nanoparticles modified with glycol chitosan. *Sci. Technol. Adv. Mater.* 13, 15002 (2012).
38. R. M. Cornell and U. Schwertmann, The Iron Oxides: Structure, Properties, Reactions, Occurrence, and Uses, VCH, Weinheim, New York (1996), p. 573.
39. R. G. López, M. G. Pineda, G. Hurtado, R. D. de León, S. Fernández, H. Saade, and D. Bueno, Chitosan-coated magnetic nanoparticles prepared in one step by reverse microemulsion precipitation. *Int. J. Mol. Sci.* 14, 19636 (2013).
40. J. Estelrich, E. Escribano, J. Queralt, and M. A. Busquets, Iron oxide nanoparticles for magnetically-guided and magnetically-responsive drug delivery. *Int. J. Mol. Sci.* 16, 8070 (2015).
41. H. Kim, Magnetoelectric Effect and Magnetodielectric Effect in Magnetic Nanoparticles, eScholarship [Internet], 2013 January [cited 2016 April]; Available from: <http://escholarship.org/uc/item/0zx5x6mc>.
42. J. Castelló, M. Gallardo, M. A. Busquets, and J. Estelrich, Chitosan (or alginate)-coated iron oxide nanoparticles: A comparative study. *Colloids Surf. Physicochem. Eng. Asp.* 468, 151 (2015).
43. D. M. Ragab and S. Rohani, Cubic magnetically guided nanoaggregates for inhalable drug delivery: *In vitro* magnetic aerosol deposition study. *AAPS PharmSciTech.* 14, 977 (2013).
44. J. Y. Yhee, S. Son, S. H. Kim, K. Park, K. Choi, and I. C. Kwon, Self-assembled glycol chitosan nanoparticles for disease-specific theranostics. *Drug Deliv. Res. Asia Pac. Reg.* 193, 202 (2014).
45. T. Srinophakun and J. Boonmee, Preliminary study of conformation and drug release mechanism of doxorubicin-conjugated glycol chitosan, via cis-aconityl linkage, by molecular modeling. *Int. J. Mol. Sci.* 12, 1672 (2011).
46. K. Kataoka, T. Matsumoto, M. Yokoyama, T. Okano, Y. Sakurai, S. Fukushima, et al., Doxorubicin-loaded poly(ethylene glycol)-poly(beta-benzyl-L-aspartate) copolymer micelles: Their pharmaceutical characteristics and biological significance. *J. Control Release Off J. Control Release Soc.* 64, 143 (2000).
47. B. Singh and V. Sharma, Influence of polymer network parameters of tragacanth gum-based pH responsive hydrogels on drug delivery. *Carbohydr. Polym.* 101, 928 (2014).
48. S. R. Jameela and A. Jayakrishnan, Glutaraldehyde cross-linked chitosan microspheres as a long acting biodegradable drug delivery vehicle: Studies on the *in vitro* release of mitoxantrone and *in vivo* degradation of microspheres in rat muscle. *Biomaterials* 16, 769 (1995).
49. S.-B. Park, J.-O. You, H.-Y. Park, S. J. Haam, and W.-S. Kim, A novel pH-sensitive membrane from chitosan—TEOS IPN; preparation and its drug permeation characteristics. *Biomaterials* 22, 323 (2001).
50. J. H. Kim, J. Y. Kim, Y. M. Lee, and K. Y. Kim, Properties and swelling characteristics of cross-linked poly(vinyl alcohol)/chitosan blend membrane. *J. Appl. Polym. Sci.* 45, 1711 (1992).
51. N. Peppas and B. Narasimhan, Mathematical models in drug delivery: How modeling has shaped the way we design new drug delivery systems. *J. Controlled Release* 190, 75 (2014).
52. R. W. Korsmeyer, R. Gurny, E. Doelker, P. Buri, and N. A. Peppas, Mechanisms of solute release from porous hydrophilic polymers. *Int. J. Pharm.* 15, 25 (1983).
53. F. S. Poletto, E. Jäger, M. I. Ré, S. S. Guterres, and A. R. Pohlmann, Rate-modulating PHBHV/PCL microparticles containing weak acid model drugs. *Int. J. Pharm.* 345, 70 (2007).

Received: 20 October 2016. Accepted: 31 December 2016.